

Ultrathin Ga₂O₃ Tunneling Contact for 2D Transition-metal Dichalcogenides Transistor

Yun Li ^{1,2}, Tinghe Yun ¹, Bohan Wei ^{1,3}, Haoran Mu ¹, LuoJun Du ², Nan Cui ^{1#}, Guangyu Zhang ^{1,2#}, Shenghuang Lin ^{1#}

1. Songshan Lake Materials Laboratory, Dongguan 523808, P. R. China.
2. Institute of Physics, Chinese Academy of Science, Beijing, 100190, P. R. China.
3. MOE Key Laboratory of Laser Life Science & Guangdong Provincial Key Laboratory of Laser Life Science, College of Biophotonics, South China Normal University, Guangzhou, 510631, China

These authors contributed equally: Yun Li, Tinghe Yun

#Corresponding author email:

Cuinan@sslslab.org.cn

zhangguangyu@sslslab.org.cn

lingshenghuang@sslslab.org.cn

KEYWORDS: ultrathin Ga₂O₃, tunneling contact, WS₂ field-effect transistors, Scalable preparation

Abstract

The development of two-dimensional (2D) transition metal dichalcogenides (TMDs) based transistors has been constrained by high contact resistance and inadequate current delivery, primarily stemming from metal-induced gap states and Fermi level pinning. Research into addressing these challenges is essential for the advancing 2D transistors from laboratory experiments to industrial-grade production. In this work, we present amorphous Ga_2O_3 as a novel tunneling contact layer for multilayer WS_2 -based field-effect transistors (FETs) to enhance electrical performance. The addition of this innovative tunneling layer avoid Schottky barrier forming while finally change into a tunneling barrier with the barrier height to just 3.7 meV, near-ideal ohmic contacts. This approach effectively reduces contact resistance to only $2.38 \text{ k}\Omega\cdot\mu\text{m}$ and specific contact resistivity as low as $3 \times 10^{-5} \Omega\cdot\text{cm}^2$. A record-high electron mobility of $296 \text{ cm}^2 \text{ V}^{-1} \text{ s}^{-1}$ and ON-OFF ratio over 10^6 are realized for WS_2 transistor at room temperature. Compared to other tunneling materials, ultrathin Ga_2O_3 layer offers scalability, cost-efficient production and broad substrate compatibility, making it well-suited for seamless integration with industrial wafer-scale electronics. A robust device performance remains highly consistent in a large-scale transistor array fabricated on $1.5 \times 1.5 \text{ cm}^2$ chips, with the average mobility closing to $200 \text{ cm}^2 \text{ V}^{-1} \text{ s}^{-1}$. These findings establish a new benchmark for contact performance in 2D transistors and prove the potential of tunneling contact engineering in advancing high-performance, scalable electronics with promising applications in quantum computing and communication.

Introduction

Two-dimensional (2D) transition metal dichalcogenides (TMDs), have emerged as leading candidates for advanced electronics and optoelectronics, owing to their high carrier mobility, tunable band gaps, and exceptional van der Waals (vdW) integrated characteristic^{1,2}. However, achieving high-quality electrical contacts remains one of the key challenges in realizing the full potential of 2D field-effect transistors (FETs) for

practical applications³⁻⁶. Conventional metal deposition techniques often result in Fermi level pinning effect at the TMD surface, which exacerbates contact resistance and prevents effective tuning of the Schottky barrier height (SBH) with different metals^{7,8}. Large Schottky barrier will impede charge injection and transport, ultimately degrading device performance⁹. Various strategies focusing on the electrodes design of metal-semiconductor (MS) structure to mitigate Schottky barrier and reduce contact resistance, for examples, applying semimetal electrodes or vdW transfer electrodes¹⁰⁻¹⁴. Different from MS structure, inserting an ultrathin insulator layer to form a metal-insulator-semiconductor (MIS) structure has proven effective in avoiding Schottky barriers via quantum tunneling meanwhile the contact mode will be dominated by the tunneling resistance¹⁵. Atomic-layer deposition (ALD) of ultrathin oxide insulator such as Ta₂O₅ has been firstly explored for this purpose, but maintaining film continuity and compactness on TMD surfaces is normally difficult can be challenging due to the dangling bond-free 2D materials surface^{16,17}. Alternative approaches have utilized 2D crystalline materials like hexagonal boron nitride (hBN), tungsten disulfide (WS₂), and multilayer InSe as tunneling layers for TMD-based FETs¹⁸⁻²⁰. The vdW stacking fabrication of these materials avoided impact from material deposition, led to significant improvements of electrical performance²¹. Although current tunneling materials have shown potential in improving transistor performance, their ability to enhance key parameters, such as mobility, remains limited and not yet sufficient for meeting the demands of industrial applications. Additionally, the scalable fabrication of these materials often introduces constraints on substrate compatibility and processing temperatures, posing challenges for seamless integration with 2D transistors and industrial-grade production of high-performance devices^{5,22,23}.

To address these limitations, we explore the use of ultrathin layer Ga₂O₃, derived from the surface of liquid gallium, as a novel tunneling contact layer. Liquid gallium cannot be completely oxidized in ambient hence represented as Ga₂O₃. This dense, amorphous layer, with a scale of more than centimeter and thickness of 2-4 nm, possess mechanical flexibility, environmental stability and, most importantly, scalability²⁴.

Additionally, the compact Ga₂O₃ film acts as a passivation layer, protecting the functional layer from Fermi level pinning and providing robust encapsulation to isolate environmental contaminants such as water and oxygen molecules^{25,26}. It can also protect transistor from external charge injection and electromagnetic interference while reduce the damage of electrostatic discharge^{27,28}. Multilayer WS₂ offers significant advantages for transistor applications, including high electronic mobility, tunable bandgap and robust thermal stability. Previous studies have also demonstrated the encapsulation effect of Ga₂O₃ on WS₂ that enhances optical performance of WS₂²⁹. Building on these findings, we focused on multilayer WS₂ transistors as a typical case to investigate the performance improvements enabled by Ga₂O₃ tunneling contacts.

We successfully demonstrate the incorporation of ultrathin Ga₂O₃ as tunneling contact layers in multilayer WS₂ (<10 layers) transistor and observe a dramatic reduction in barrier height from 258 meV to just 3.7 meV. Notably, the transistor approaches the ideal of ohmic contact since the contact resistance of the transistor is largely influenced by the tunneling resistance. The final specific contact resistivity (ρ_c) falls within the range of 3-25 $\times 10^{-5} \Omega \cdot \text{cm}^2$. Highest carrier mobility up to 296 $\text{cm}^2 \text{V}^{-1} \text{s}^{-1}$ at room temperature is achieved with tunneling contact, which is a record-high value for multilayer WS₂-based transistors, to the best of our knowledge²¹. Our results also show consistent performance of a transistor array across a $1.5 \times 1.5 \text{ cm}^2$ chip, attributed to the high quality and uniformity of large-area printed ultrathin Ga₂O₃ layer. These findings demonstrate the exceptional potential of ultrathin amorphous Ga₂O₃ as an effective tunneling contact layer for 2D semiconductor devices. By addressing both performance and scalability challenges, this strategy enhances the practical application and commercial viability of 2D semiconductor technologies.

Results

Large-scale contact layer preparation and characterization

Ultrathin Ga₂O₃ layer was synthesized by printing of native oxide onto a variety of substrates³⁰. The printing installation and oxide printing process of Ga₂O₃ tunneling

layer was illustrated in **Fig. 1a**. The polypropylene carbonate (PPC) spin-coated on polydimethylsiloxane (PDMS) serves as the desired substrate. The liquid metal forms an oxide-coated meniscus that bridges the gap between the printer head and the substrate. As the substrate moves, an ultrathin Ga₂O₃ layer is deposited with minimal residual metal. The film was then transferred on top of WS₂ nanoflakes with the association of PPC as detailed in Supplementary **Fig. S1** and the supporting notes. **Fig. 1b** demonstrates a 3D diagram of tunneling contact transistor assembly structure, while gold (Au) electrodes are insulated from WS₂ nanoflake by the ultrathin Ga₂O₃ layer. In the tunneling contact device, current will firstly be tunneling beyond the tunneling layer and then transfer in channel material when a bias voltage is applied on source and drain electrodes.

To facilitate a direct comparison within a single device, Au electrodes were deposited on both the Ga₂O₃ and WS₂ surfaces, with a channel length (L_{CH}) of 4.5 μm and width (L_{CW}) of 20 μm , as depicted in the optical image in **Fig. 1c** (top). The ultrathin Ga₂O₃ layer formation is characterized as a self-limiting oxidation process, producing a dense film that protects the transistor channel from environmental factors and prevents further oxidation²⁶. Supplementary **Fig. S2a** displayed photographs of ultrathin Ga₂O₃ layer printed on PDMS and PPC surface and then transferred on SiO₂/Si substrates, highlighting the versatility and adaptability of the process. These photos showcased the uniformity and continuity of Ga₂O₃ layers with no-selectivity of substrate, essential for achieving large-area transistor arrays on chips.

Despite variations in film thickness due to different oxidation time in ambient as well as synthesis methods, no correlation with device performance was observed. Specifically, the Ga₂O₃ film measured 2.6 nm in thickness for tunneling layer (**Fig. 1c**, bottom). The WS₂ nanoflakes is less than 10 layers (Supplementary **Fig. S2b**). The printed film has a metallic character that can oxidize over time and finally the gallium oxide tunneling layers with stoichiometric ratios approaching 2:3 can be formed, which was verified by X-ray photoelectron spectroscopy (XPS) test (Supplementary **Fig. S2c**). The XPS results confirm the successful formation of Ga₂O₃ with gallium predominantly in the Ga³⁺ oxidation state. The Ga 3d peak (~20.0–21.0 eV) and Ga 2p peak (1117–

1118 eV) both exhibit symmetric shapes, indicating the absence of metallic Ga or other lower oxidation states. In the O 1s spectrum, the primary peak (530.1–531 eV) corresponds to lattice oxygen (O^{2-}) in the Ga_2O_3 structure. These results confirm the high purity and stable composition of the Ga_2O_3 layer, with only minimal surface contamination.

Raman spectra of the WS_2 nanoflake, shown in **Fig. 1d**, identified primary peaks at $2LA(M)$, $E''(M)$, $E_{2g}^1(\Gamma)$, and $A_{1g}(\Gamma)$ represent for the longitudinal acoustic mode and in-plane vibrational mode at the M point, in-plane vibrational mode and out-of-plane vibrational mode at the Gamma point from WS_2 , respectively. The consistency in peak positions and full-width at half-maximum (FWHM) before and after Ga_2O_3 encapsulation indicated negligible strain or doping introduced during the process. Photoluminescence (PL) spectra (**Fig. 1e**) revealed a slight increase in exciton energy for Ga_2O_3/WS_2 , with a 0.012 eV shift, attributed to dielectric screening from Ga_2O_3 film. These results confirmed the effective encapsulation of Ga_2O_3 layer, demonstrating its ability to maintain the stability and performance of WS_2 -based transistors potential for reliable protection in electronic applications.

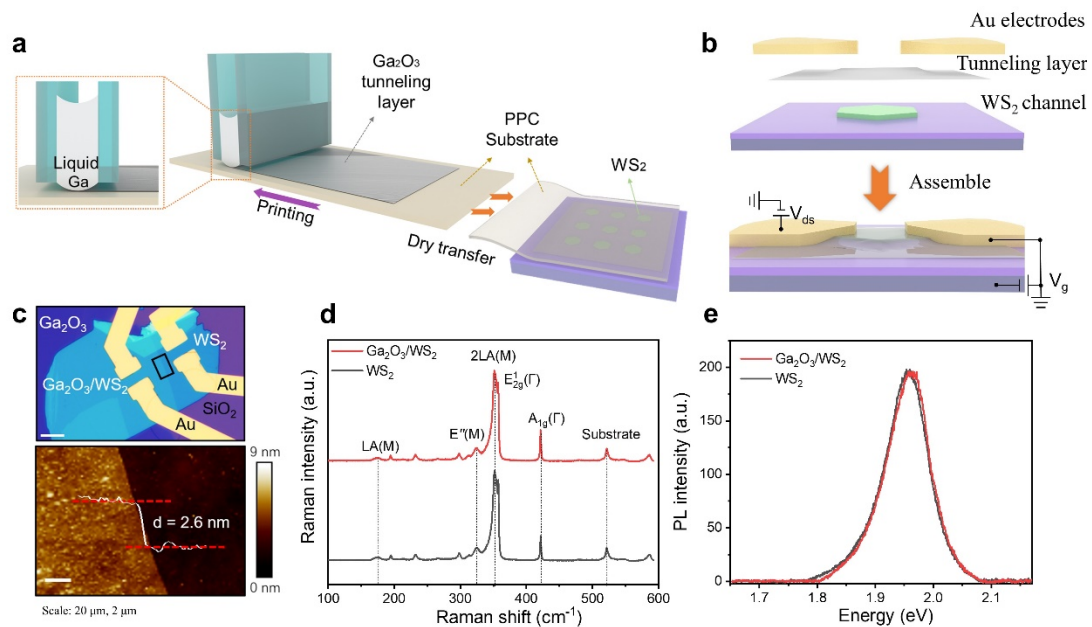


Fig. 1 | Device Structure and Characterization (a) Schematic image of printing setup illustrating the continuous ultrathin Ga_2O_3 tunneling layer on to PPC-coated PDMS

substrate. **(b)** 3D diagram of tunneling contact transistor assembly structure. Ultrathin Ga₂O₃ tunneling layer separates the gold electrodes from the WS₂ channel material. SiO₂ (300 nm thickness) work as the dielectric layer. **(c)** Optical micrographs of the Ga₂O₃/WS₂ tunneling contact transistor (top) and atomic force micrographs (AFM) of Ga₂O₃ (bottom), showing a thickness of Ga₂O₃ layer is 2.6 nm. Scale bar: 20 μm (top) and 2 μm (bottom). **(d)** Raman spectra of both the WS₂ and Ga₂O₃/WS₂ regions, exhibiting no obvious wavenumber shift. **(e)** PL spectra of the WS₂ and Ga₂O₃/WS₂ regions with 0.01 eV peak shift.

Enhanced electrical performance of WS₂ FETs with Ga₂O₃ tunneling layer

To evaluate the potential of the Ga₂O₃ tunneling layer in enhancing the performance of WS₂-based FETs, electrical tests were conducted under various conditions. **Fig. 2a** presents the typical room-temperature transfer curves for a Ga₂O₃/WS₂ transistor tested in vacuum as the drain–source current (I_{ds}) changed with drain-source bias (V_{ds}) varying from 0.01 V to 1 V. An ultra-high electronic mobility (μ_e) could achieve 263 cm² V⁻¹ s⁻¹ at $V_{ds} = 1$ V. Building on this initial result, we performed extensive device fabrication and repeated testing. Through these experiments, the highest recorded mobility reached 296 cm² V⁻¹ s⁻¹ with a ON-OFF current ratio above 10⁶, with the logarithmic form of transistor showed in insert figure of **Fig. 2a**. The morphology and the corresponding transfer curve of this device were provided in Supplementary **Fig. S3**, demonstrating the reliability and consistency of our fabrication process. Meanwhile, the output characteristics (**Fig. 2b**) displayed linear I_{ds} - V_{ds} behavior over a range of $V_{ds} = 0\sim 3$ V, indicating the presence of ohmic contacts.

Compared to WS₂-FETs, Ga₂O₃/WS₂ transistor demonstrated significant improvements in both ON-state current and mobility. The comparison experiment, including transfer and output results, are displayed in Supplementary **Fig. S4**. All transistors showed the typical n-type characteristic. Notably, the ON-OFF ratio of Ga₂O₃/WS₂ transistor increased by an order of magnitude compared to the WS₂ transistor. The maximum μ_e increase from 68.67 cm² V⁻¹ s⁻¹ of WS₂ transistor to 212.84 cm² V⁻¹ s⁻¹ to Ga₂O₃/WS₂ transistor under ambient condition, and from 101.23 cm² V⁻¹

s^{-1} to $253.97 \text{ cm}^2 \text{ V}^{-1} \text{ s}^{-1}$ in vacuum. It is worth noting that the output curve of WS_2 transistor exhibited noticeable nonlinearity above V_{ds} of 0.5 V, suggesting the formation of Schottky contact between multilayer WS_2 and deposited Au electrodes. In contrast, the Ga_2O_3 tunneling layer enabled a linear output response, confirming a significant reduction in the Schottky barrier and the establishment of ohmic contacts.

The improved electrical performance, including increased mobility and a highly linear output, is attributed to the tunneling contact provided by the Ga_2O_3 layer. Firstly, according to quantum mechanical principles, electrons can tunnel through an energy barrier even when their energy is lower than the barrier height. When a thin Ga_2O_3 layer is inserted between metal electrodes and WS_2 , it attenuates the electron wave function of the metal, reducing its penetration into the semiconductor and thus lowering the SBH. Additionally, the interface between Ga_2O_3 and WS_2 forms a dipole due to differences in charge neutrality levels, preventing the built-in shift of Fermi levels and further reducing the Schottky barrier^{17,21}.

In addition to enhancing the electrical performance of transistors through tunneling contacts, the encapsulation function of Ga_2O_3 can be demonstrated by comparing device performance under ambient and vacuum conditions. Transconductance, a key performance index directly related to the amplification ability and current control efficiency of transistors, can be one representation to reflect this effect. **Fig. 2c** illustrates the variation in transconductance for WS_2 transistors and $\text{Ga}_2\text{O}_3/\text{WS}_2$ transistors under both ambient and vacuum conditions, with data extracted from Supplementary **Fig. S4c** and **S4f**. The $\text{Ga}_2\text{O}_3/\text{WS}_2$ transistor consistently achieved significantly higher transconductance across all on-state conditions, a result that aligned with the previously noted improvements in mobility. Moreover, transconductance measured in vacuum consistently exceeds that in ambient conditions for both transistors. Factors such as oxide etching, charge trapping, parasitic capacitance, and noise from air molecules usually affect transistors operating in ambient conditions^{31,32}. This effect is particularly pronounced in transistors without encapsulation, explaining the substantial difference in transconductance for the WS_2 transistor, which increased from 3.1 mS in ambient to 13.5 mS in vacuum at $V_{\text{gs}} = 40 \text{ V}$, representing a 335.5%

improvement. Therefore, an effective encapsulating layer is highly desired for the practical applications of 2D devices. For the Ga₂O₃/WS₂ transistor, where Ga₂O₃ also served as an encapsulating layer, protection from the influence of air molecules. The difference of transconductance could be mainly considered due to the variation of heat dissipation efficiency. Consequently, the increase in transconductance from ambient (29.1 mS) to vacuum (37.3 mS) was only 28.4%. These findings demonstrate the encapsulation effect of Ga₂O₃, ensuring stable transistor performance under ambient conditions.

Fig. 2d benchmarks the performance of the Ga₂O₃/WS₂ transistor, comparing its mobility and ON-OFF ratio against other reported values for multilayer WS₂ transistor. Our Ga₂O₃/WS₂ transistor demonstrated the highest mobility levels close to 300 cm² V⁻¹ s⁻¹. This performance surpasses that achieved by other enhancement methods such as chemical doping^{33–35} or plasma treatment³⁶ of WS₂ channel materials, dielectric layer design^{37,38}, and other contact engineering techniques^{21,39–41}. Additionally, the ON-OFF ratio of our device is also relatively high compared to other WS₂-based transistors reported in the literature.

The transfer length method (TLM) measurement is typically used to measure the contact resistance of metal-semiconductor contacts. However, when conductors are separated by a thin insulating layer, the tunneling current and voltage along the contact length show spatial variations. The magnitude of tunneling resistance is directly related to the contact area in the longitudinal direction, where the larger contact areas result in lower tunneling resistance. In the transverse direction, the contact length becomes relevant after electrons tunnel through the tunneling layer. When the tunneling layer is uniform, sufficiently thin, and free of charge trapping effects, calculations can be simplified⁴². To facilitate performance comparisons with existing tunneling contact 2D transistors, we also employ the TLM method to characterize the specific contact resistivity of Ga₂O₃/WS₂ device, as the configuration shown in Supplementary **Fig. S5a**. The contact distances varied in a gradient from 2 μm to 28 μm. When current flows through the contact, each contact presents a voltage drop due to contact resistance, while current flow through the semiconductor creates a voltage drop due to body

resistance. By plotting the resistance values against the contact distances, the contact resistance can be obtained from the Y-axis intercept, and the slope represents the body resistance. **Fig. 2e** shows the I_{ds} - V_{ds} relationship for source-drain electrodes with different spacings in the $\text{Ga}_2\text{O}_3/\text{WS}_2$ device at $V_{gs} = 80$ V. All measurements exhibited good linearity, allowing the total resistance value to be determined by fitting the slope of the I - V linear relationship. Then the specific contact resistivity for contact of $\text{Ga}_2\text{O}_3/\text{WS}_2$ transistor was extracted and the data are shown in **Fig. 2f**. Contact area of electrodes and Ga_2O_3 tunneling layer was defined as $20 \mu\text{m} \times 10 \mu\text{m}$. Finally, ρ_c falls within the range of $\sim 3\text{-}25 \times 10^{-5} \Omega \cdot \text{cm}^2$. This low resistivity could be attributed to the tunneling effect of the Ga_2O_3 layer and preventing Fermi level pinning with an excellent van der Waals contact. When compare to the traditional deposition metal electrode, the total contact resistance for the WS_2 transistor was significantly reduced from $32.52 \text{ k}\Omega \cdot \mu\text{m}$ (Au electrodes) to $2.38 \text{ k}\Omega \cdot \mu\text{m}$ (Ga_2O_3 tunneling contacts). The detailed fitting results for both deposited Au-contacts and Ga_2O_3 tunneling contacts are shown in Supplementary **Fig. S5b**. Consequently, the achieved contact resistance is within the range of ideal ohmic contacts and is among the lowest reported for WS_2 FETs with various contact engineering techniques (Supplementary **Fig. S5c**)^{11,21,39–41,43}. It indicates the potential of Ga_2O_3 tunneling being applied to the actual use scenario of electronic devices.

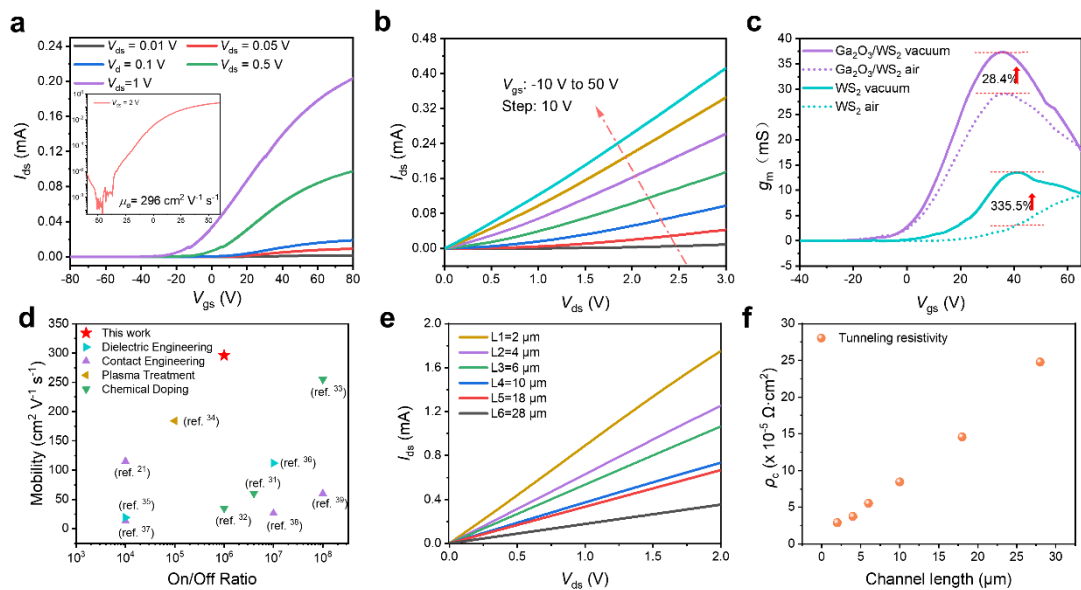


Fig. 2| Room Temperature Electrical Characterization (a) I_{ds} - V_{gs} transfer

characterization of the Ga₂O₃/WS₂ tunneling contact transistor under vacuum conditions ($\sim 10^{-4}$ Pa). Inset: The logarithm representation of transfer curve of the device with the recorded highest mobility, measured under $V_{ds} = 2$ V. **(b)** I_{ds} - V_{ds} output characterization of the Ga₂O₃/WS₂ tunneling contact transistor with V_{gs} changes from -10 V to 50 V in step of 10 V. **(c)** Transconductance of Ga₂O₃/WS₂ tunneling device and WS₂ device under air condition and vacuum. $V_{ds}=0.01$ V. **(d)** Comparison of mobility with other multilayer WS₂ based FETs. **(e)** Resistance of the Ga₂O₃/WS₂ tunneling contact transistor channel at different contact distances. **(f)** Plot of the specific contact resistivity ρ_c as a function of channel length.

Barrier height comparison

The contact resistance in transistors is primarily influenced by tunneling resistance and the barrier height. To gain deeper insights into the operating behavior of the Ga₂O₃/WS₂ transistor and to highlight its differences from pristine WS₂, we systematically conducted transport measurements at various temperatures. **Fig. 3a** and **3d** illustrate the temperature-dependent transfer characteristics of the Ga₂O₃/WS₂ and WS₂ transistors, respectively, as the temperature decreases from room temperature to 90 K. As the temperature decreases, the resistivity of the channel material decreases, primarily due to diminished phonon scattering, which enhances electron mobility⁴⁴. In contrast, the contact resistance increases with cooling. According to the thermionic emission theory, lower temperatures make it more difficult for electrons to overcome the barrier from the metal contact into the semiconductor. This increase in contact resistance is particularly pronounced at low V_{gs} , where the lower concentration of charge carriers results in a higher dependence on the thermionic emission process for current flow¹⁸. At high V_{gs} , the increased gate bias induces a greater concentration of charge carriers at the semiconductor surface, which can help to mitigate the effect of the contact resistance by enhancing the tunneling effect and facilitating more efficient current flow. The interplay of these factors leads to complex temperature-dependent conductivity in transistors, often resulting in a metal-insulator transition (MIT)⁴⁵. This principle explains the observed crossover from an insulating to a metallic regime, occurring

around $V_{gs} \approx 60$ V for Ga₂O₃/WS₂ transistor and around $V_{gs} \approx 20$ V for WS₂ transistor.

The temperature-dependent mobility of both Ga₂O₃/WS₂ and WS₂ transistors, calculated from their metallic regimes, are presented in **Fig. 3b** and **3e**, respectively. As the temperature decreased from room temperature to 90 K, the field-effect mobility of the Ga₂O₃/WS₂ transistor showed a continuous increase, reaching approximately 1800 cm² V⁻¹ S⁻¹, while the WS₂ transistor only achieved 103 cm² V⁻¹ S⁻¹ at 90 K. This exceptionally high mobility at low temperatures is unprecedented among other methods^{46,47}. In the high temperature regime, the mobility follows the expression $\mu_{FE} \propto T^{-\gamma}$, where lattice vibrations intensify, leading to more frequent electron-phonon scattering events. The temperature damping factor γ characterizes the severity of mobility dependency on temperature, which was found to be 1.32 for the WS₂ transistor and 2.48 for the Ga₂O₃/WS₂ transistor. This behavior was consistent across devices incorporating the same Ga₂O₃ tunneling layer, as demonstrated in Supplementary **Fig. S6**. The difference in the γ exponent between the Ga₂O₃/WS₂ and WS₂ transistors can be attributed to several factors. One possibility is the fundamental difference in charged-impurity scattering compared to WS₂ alone, leaving phonon scattering as the dominant mechanism at high temperatures^{48,49}; Additionally, the encapsulation effect of the ultrathin Ga₂O₃ layer, with its superior interface engineering, minimizes structural damage and reduces scattering from material imperfections, contributing to the observed high mobility and unique temperature dependence.

To precisely determine the barrier height of the tunneling contact, Arrhenius plots ($\ln(I_{DS}/T^{1.5})$ versus $1000/T$) were extracted from the temperature-dependent transport measurements, as shown in Supplementary **Fig. S7a** and **S7b** for Ga₂O₃/WS₂ and WS₂ respectively. According to thermionic emission theory, the current in the subthreshold region is primarily governed by thermally assisted tunneling and thermionic emission, which can be described by the equation:

$$I_{ds} = A_{2D}^* T^{3/2} \exp\left(-\frac{q\phi_B}{k_B T}\right) \left[1 - \exp\left(-\frac{V_{ds}}{k_B T}\right)\right] \quad (1)$$

where $A_{2D}^* = \frac{q(8\pi k_B^3 m^3)^{0.5}}{h^2}$ is the Richardson constant for a 2D system, h is the

Planck constant, m is the electron effective mass, T is the temperature, k_B is Boltzmann's constant, q is the elementary charge, and ϕ_B is the effective contact barrier height for a given gate-source voltage^{50,51}. In Schottky barrier devices, the inverse subthreshold slope is influenced by thermally assisted tunneling, and the tunneling current becomes negligible only when the gate voltage drops below the flat band voltage (V_{FB}). This is crucial for accurately determining the barrier height at this specific gate voltage. By analyzing the slope of the curves in the high-temperature range using the simplified equation (2) derived from equation (1)⁵², the gate voltage-dependent ϕ_B values were collected and presented with error bars in **Fig.3c and 3f**.

$$\ln (I_{ds}/T^{1.5}) = \frac{-\phi_B}{k_B T} + c \quad (2)$$

At relatively low gate voltage, the effective barrier height displays a linear response to V_{gs} , indicating that the current is primarily dominated by thermionic emission. As the gate voltage increases, a deviation from this linear trend signifies the commencement of significant thermally assisted tunneling. The flat band voltage is determined by identifying the data point where the linear trend begins to deviate, making it possible to pinpoint the accurate barrier height determination. For the Ga₂O₃/WS₂ transistor, the barrier height at V_{FB} was determined to be 3.7 meV, while for the WS₂ transistor, it was 258 meV. This substantial reduction in barrier height for the Ga₂O₃/WS₂ transistor, by two orders of magnitude validated the formation of ohmic contacts. This significant reduction could be attributed to the tunneling contact effect of Ga₂O₃ layer, thereby minimizing the interaction between the metal and the semiconductor and the forming of Schottky barrier. It not only attenuated the metal electron wave function but also mitigated the Fermi level pinning effect. Together, these mechanisms contributed to the superior electrical performance observed in devices incorporating the Ga₂O₃ tunneling layer.

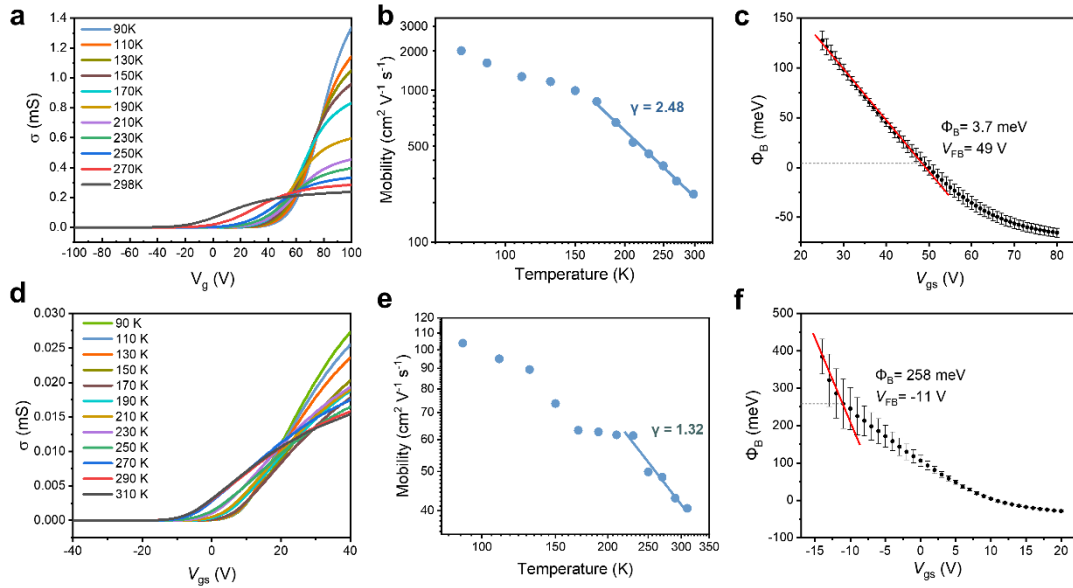


Fig. 3 | Temperature Dependence of Transport Characteristics. Low temperature transfer curve of (a) Ga₂O₃/WS₂ tunneling contact transistor and (d) WS₂ transistor at $V_{ds} = 1$ V. Both of device exhibited metal-insulation transition. Temperature-dependent mobility of (b) Ga₂O₃/WS₂ tunneling contact transistor and (e) WS₂ transistor. At high temperature region is typically phonon scattering. The exponent γ was 2.48 for the tunneling contact and 1.32 for the Au-contact. Schottky barrier heights of the (c) Ga₂O₃/WS₂ tunneling contact transistor and (f) WS₂ transistor. The barrier height had largely reduction from 258 meV to 3.7 meV with the insert of Ga₂O₃ tunneling layer.

Low temperature output and tunneling mechanism

To gain a deeper understanding of the tunneling mechanism facilitated by the insertion of the ultrathin Ga₂O₃ layer, we examined the Fowler–Nordheim (F–N) tunneling and direct tunneling (DT) models in relation to the transport characteristics of the Ga₂O₃/WS₂ transistor. We first explored the key distinctions between of tunneling model, as the schematic energy band diagrams for both illustrated in **Fig. 4a**. According to quantum theory, if the potential barrier is sufficiently thin, the electron wave function can traverse it, leading to a non-zero probability of electrons appearing on the opposite side of the barrier. When a strong electric field is applied, F-N tunneling occurs, enabling the electron wave function to penetrate the triangular barrier and enter the conduction band of the dielectric material. Conversely, when the voltage across the

insulating layer is low, electrons traverse the full thickness of the oxide, making the gate current dependent on direct tunneling⁵³. It normally occurs with nano-thickness dielectric layer. In this context, the F-N and DT models can be described as follows:

$$\text{F-N tunneling:} \quad \ln\left(\frac{I_{ds}}{V_{ds}^2}\right) = \ln\left(\frac{Aq^3m_0}{8\pi h\Phi_B d^2 m^*}\right) - \frac{8\pi\sqrt{2m^*}\Phi_B^{3/2}d}{3hqV_{ds}} \quad (3)$$

$$\text{Direct tunneling:} \quad \ln\left(\frac{I_{ds}}{V_{ds}^2}\right) = \ln\left(\frac{Aq^2\sqrt{2m^*}\Phi_B}{V_{ds}h^2d}\right) - \frac{4\pi\sqrt{2m^*}\Phi_B}{h} \quad (4)$$

where A is the electrical contact area, d is the barrier width, h is Planck's constant, m^* is the effective mass of an electron in the WS₂ flake ($0.33 m_0$, where m_0 is the rest mass), and Φ_B is the barrier height⁵⁴.

The output curve of the Ga₂O₃/WS₂ transistor at $V_{gs} = 80$ V continued to exhibit excellent linearity as the temperature decreases, as shown in **Fig. 4b**. This further verified the formation of an ohmic contact due to the Ga₂O₃ tunneling layer. Only a slight deviation from linearity was observed when the temperature drops below 100 K, which might be attributed to the increasing contact resistance at low temperatures. Based on the output results, a plot of $\ln(I_{ds}/V_{ds}^2)$ as a function of $1/V_{ds}$ was displayed in **Fig. 4c**. The curves exhibited a logarithmic dependence across all temperatures, rather than the linear dependence expected for F-N tunneling. This suggested that there was no significant evidence of F-N tunneling, even at higher voltage biases. Instead, DT Fitting demonstrated a linear relationship when $\ln(I_{ds}/V_{ds}^2)$ was plotted against $\ln(1/V_{ds})$, as exhibited in **Fig. 4d**, with the slope of the fitted line being close to 1. This nearly perfect fit to the DT model equation (4), indicating that the charge carrier injection in the Ga₂O₃/WS₂ transistor was dominated by direct tunneling. Direct tunneling leverages quantum effects and can play a crucial role in emerging technologies such as quantum computing and quantum communication. Unlike F-N tunneling, direct tunneling does not rely on high electric fields to reduce the barrier, which allows devices to operate with lower power consumption, faster response times, and reduced heat generation. This explains the exceptional electrical performance of the Ga₂O₃/WS₂ transistor with the Ga₂O₃ tunneling layer and highlights its potential for future applications in advanced electronic circuits. By applying the fitting equation, the DT barrier parameter ($d\sqrt{\Phi_B}$), which quantifies the ease with which electrons can

tunnel through the Ga₂O₃ barrier, was found to vary in the range of 0.025 - 0.032 meV^{1/2}·nm across the temperature range of 77.5 to 300 K, as shown in Supplementary **Fig. S8**. Although the Ga₂O₃ tunneling layer was thicker than previously studied hBN layers, the barrier parameter for Ga₂O₃ tunneling contacts is significantly lower than that of hBN ²¹. This relatively low range indicated that the Ga₂O₃ tunneling layer provided a more efficient tunneling pathway compared to other materials like hBN or metal formed junctions ⁵⁵, thereby contributing to the observed high performance of the Ga₂O₃/WS₂ transistor. It further confirmed that the addition of the Ga₂O₃ tunneling layer leads to a substantial reduction in the barrier height.

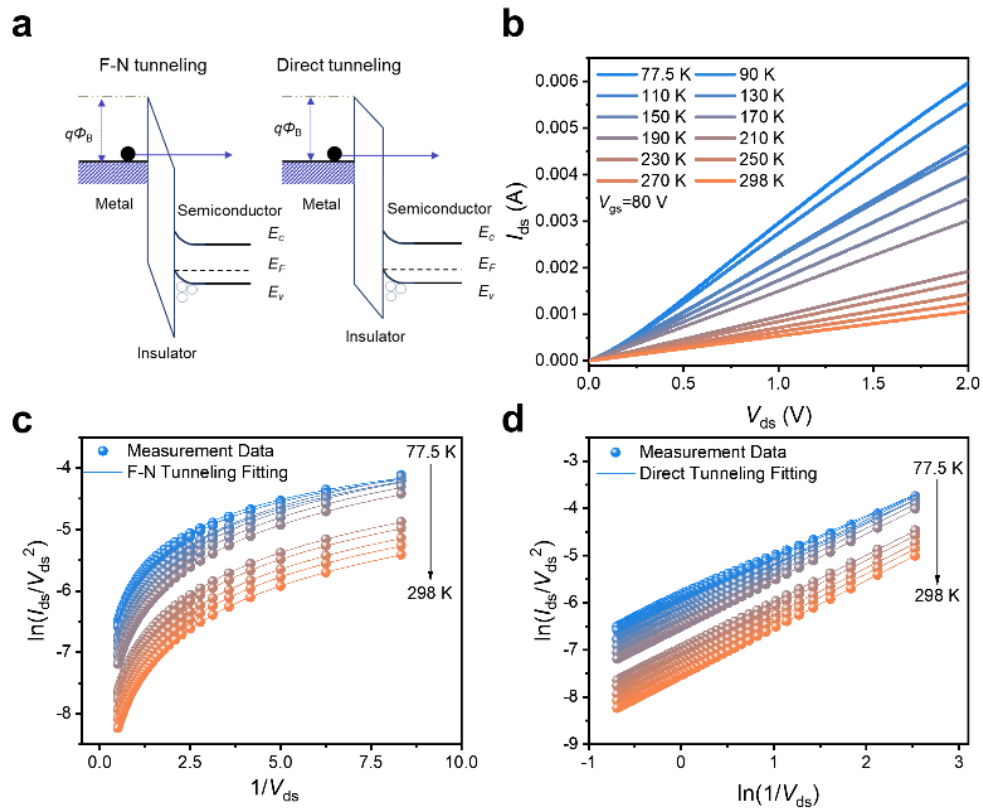


Fig. 4| Tunneling Mechanism Analysis. (a) The schematic energy band diagrams for Fowler-Nordheim tunneling and direct tunneling. (b) Output curve with temperature decrease. Linear output displayed at all temperature especially above 90 K. (c) Fowler-Nordheim tunneling fitting with temperature dependent output data. Dash lines show logarithmic relations fitted to the data. (d) Direct tunneling fitting with temperature dependent output data. Dash lines display good linear fit.

Scalability and Reproducibility of Ga₂O₃/WS₂ FETs

Building upon the low-cost, large-area scalable fabrication of ultrathin Ga₂O₃ layer, we explored the potential for creating scalable transistor arrays on single chip. By leveraging the uniform and high-quality properties of the printed Ga₂O₃ films, we successfully fabricated an extensive array of Ga₂O₃/WS₂ FETs, demonstrating the feasibility of this approach for large-scale device integration³⁰. The following sections detail the experimental results obtained from these arrays which exhibit impressive performance metrics and consistency across a wide substrate area. **Fig. 5a** illustrated the layout of Ga₂O₃/WS₂ FET arrays fabricated on a 1.5 x 1.5 cm² SiO₂/Si chip. The multilayer WS₂ nanoflakes, obtained through exfoliation, had controlled thickness less than ten layers to ensure uniform electrical properties of the channel material. These nanoflakes were evenly distributed across the entire substrate. A large-area Ga₂O₃ film was then covered on all WS₂ nanoflakes, followed by deposition of Au electrodes.

The electrical characteristics of the Ga₂O₃/WS₂ FETs were displayed in **Fig. 5b** and **5c** with the transfer curve measured under a V_{ds} of 1 V. The linear transfer characteristics, where the I_{ds} increased linearly with the V_{gs} over a wide range, indicated the formation of high-quality ohmic contacts and effective gate modulation for all transistor arrays. Meanwhile, the logarithmic representation of the transfer characteristics revealed the good repeatability of high ON-OFF current ratio (all exceeding 10^6), which is crucial for digital switching applications. The experimental results indicate that channel material was heavily doped, primarily due to the intrinsic quality of the WS₂, which also leads to the higher subthreshold slope. This observation is consistent with the transfer characteristics measured separately for WS₂ (Supplementary **Fig. S4**). Additionally, most encapsulated WS₂ devices maintained stable performance for over three weeks, with less than 20% reduction in mobility, as shown in **Fig. 5d**. The variation of mobility $\Delta\mu$ was defined as $\mu - \mu_0$, where μ_0 was the initial mobility and μ was for the mobility measured after a period of time. The error bar was calculated with the statistics of 11 devices, ensuring the reliability of our stability measurement. The variation of ON-OFF ratio also maintain within an order of magnitude after three weeks, indicating that good switching characteristics were still retained in Ga₂O₃/WS₂

transistor. These results demonstrated the effectiveness of Ga₂O₃ encapsulation in preserving the electrical properties of WS₂ over time while acting as a tunneling layer.

The electrical parameter of 25 transistors, including mobility and ON-OFF ratio, were collected and statistically analyzed. **Fig. 5e** presented a histogram of mobility, which followed a relatively Gaussian distribution, with an average μ_e of 191 cm² V⁻¹ s⁻¹ \pm 43.5 cm² V⁻¹ s⁻¹. The standard deviation (σ) and correlation coefficient (R^2) from the fitting process supported the high confidence of statistics. All achieved mobilities were significantly higher than those typically reported for WS₂ transistors without tunneling contacts. It demonstrated the reproducibility and reliability of the Ga₂O₃ tunneling contact approach, which is essential for scalable electronics. The corresponding ON-OFF ratio distribution, with most devices exhibited values between 10⁶ and 10⁸ (**Fig. 5f**). Such high ON-OFF ratios are indicative of excellent switching performance, being appropriate for low-power and high-speed electronic applications. These statistical results validated the scalability and reproducibility of Ga₂O₃ as a tunneling contact layer, demonstrating its practical value and significance for industrial and commercial applications in 2D semiconductor electronic devices. Specifically, the printed Ga₂O₃ layer offers significant advantages over other tunneling layer materials in integrating with large-area grown WS₂ nanolayer. This synergy enables the formation of industrial-scale device arrays, where Ga₂O₃ serves as an efficient tunneling contact layer. Its compatibility with large-scale WS₂ film deposition techniques facilitate the production of uniform and high-performance electronic devices, making it a promising candidate for the development of scalable and commercially viable semiconductor technologies.

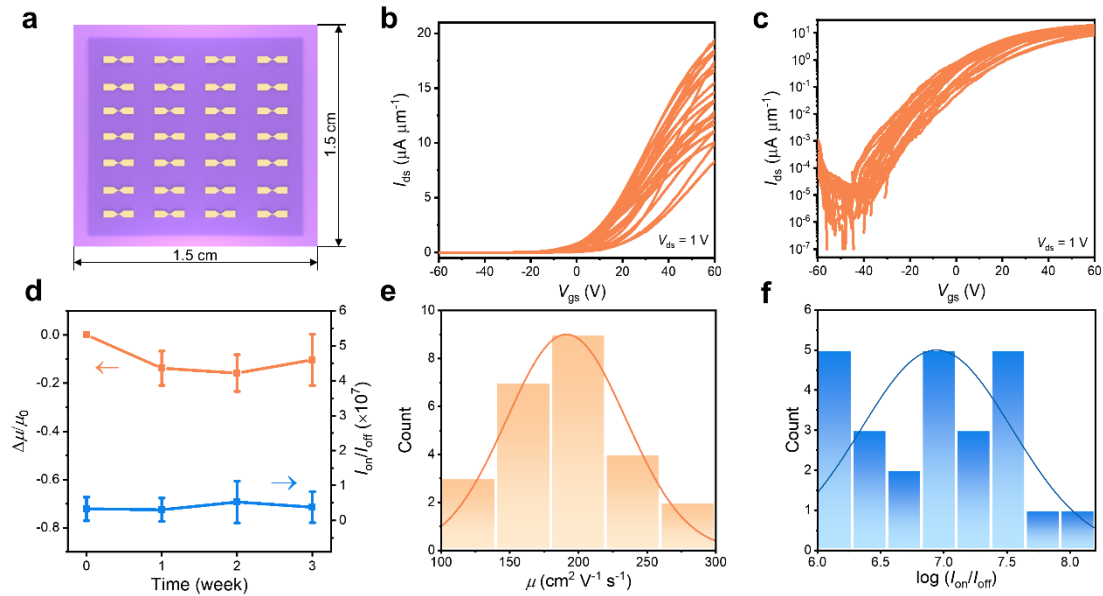


Fig. 5 | Statistics of scaled devices. (a) Schematic diagram of Ga₂O₃/WS₂ FET arrays fabricated on 1.5 x 1.5 cm² SiO₂/Si chip. Deep purple region represents for Ga₂O₃ layer. (b) linear representation and (c) Logarithmic representation of the transfer characteristics of Ga₂O₃/WS₂ FETs with L_{CH} of 4.5 μm and L_{CW} of 6 μm, under $V_{ds} = 1$ V. (d) Long time stability of FETs for three weeks measurement. The variation of mobility $\Delta\mu = \mu - \mu_0$. The variation of ON-OFF ratio after weeks were presented as I_{on}/I_{off} . The error bar represent for statistics of devices. (e) Histograms showing the variation in electron mobility for Ga₂O₃/WS₂ FETs. A total of 25 transistors were tested and counted. (f) Histograms of corresponding ON/OFF ratio of transistors.

Conclusion

In this study, we have demonstrated the success of ultrathin amorphous Ga₂O₃ layer as tunneling contact layers for WS₂-based FETs. Our findings revealed that the incorporation of Ga₂O₃ significantly reduced the barrier height from 258 meV to 3.7 meV, approaching ideal ohmic contact conditions. The Ga₂O₃ layer also acted as an effective passivation layer, protecting the WS₂ channel from environmental contaminants and maintaining device stability. The Ga₂O₃/WS₂ transistors exhibited superior electrical performance, including ultra-high electron mobility of up to 296 cm² V⁻¹ s⁻¹ at room temperature and low specific contact resistivity within range of ~ 3-25

$\times 10^{-5} \Omega \cdot \text{cm}^2$. These results surpassed those obtained from traditional contact engineering methods. Different from other tunneling layer, the scalable and low-cost fabrication of Ga_2O_3 films is particularly advantageous for practical electronic device manufacturing. Overall, the introduction of Ga_2O_3 as a tunneling contact layer not only addresses the challenges of high contact resistance and poor environmental stability in 2D semiconductor devices at the same time, but also opens new avenues for the development of high-performance, scalable, and industrial-grade electronics.

Methods

Materials Preparation

WS_2 nanoflakes were mechanically exfoliated from a single crystal (purchased from HQ Graphene) and transferred onto a SiO_2/Si substrate with a 300 nm thick SiO_2 layer. A printer head was assembled using two glass slides with a 2 mm gap. Liquid gallium (Sigma-Aldrich, 99.99% trace metal basis) sources were melted and injected into the printer head using a syringe. PPC substrates were prepared by spin coating the solution onto the desired PDMS substrates. The printer head was positioned close to the target substrate until the liquid metal meniscus contacted the surface. The printing process was initiated by translating the substrate at a controlled speed to achieve uniform printing. The preparation process of large area Ga_2O_3 was shown in the appendix video.

Device Fabrication

A clean, continuous region of the Ga_2O_3 layer, free from gallium residues, was selected. Using a dry-transfer platform, the Ga_2O_3 film was transferred onto the WS_2 nanoflakes with the aid of PPC layer as the transfer medium. The residual PPC was removed using acetone, leaving WS_2 nanoflakes covered with the Ga_2O_3 layer. $\text{Ga}_2\text{O}_3/\text{WS}_2$ back-gated FETs were fabricated using photolithography to pattern the electrodes, followed by the deposition of 50 nm thick Au electrodes through thermal evaporation and lift-off processes.

Materials Characterization

The thickness of each layer was measured using AFM (Bruker/Dimension Icon). Optical properties were analyzed using Raman spectroscopy and photoluminescence spectroscopy (LabRAM HR800, Horiba Jobin-Yvon) with a 532 nm excitation wavelength. Laser power was adjusted to approximately 1 mW to ensure consistent excitation conditions for samples exposed to air for different durations. The signals were captured for 1 s and accumulated over three measurements. XPS analysis was performed on SiO₂/Si substrates using a Thermo Scientific K-Alpha XPS spectrometer, equipped with a monochromatic Al K α source and a concentric hemispherical analyzer (CHA) to determine the chemical composition.

Electrical Characterization

All electrical characterizations were performed at room temperature in a high-vacuum environment ($\sim 10^{-4}$ Torr) using a Keysight B1500A semiconductor parameter analyzer. Standard DC sweeps were used to measure the transfer and output characteristics of all devices. To stabilize the FETs, each device underwent multiple repetitions of the same measurement. Transfer characteristics were measured three times for conditioning, with the fourth measurement used for analysis. Output characteristics were measured twice after the transfer characteristics, with the second measurement used for analysis.

Acknowledgements

Y. Li. and T. Yun contributed equally to this work. We acknowledge the support from the National Natural Science Foundation of China (No. 62204165), Guangdong Basic and Applied Basic Research Foundation (No. 2021B1515120034), National Key R&D Program of China (No. 2021YFA1202902), the National Natural Science Foundation of China (No. 12204336), and Songshan Lake Materials Laboratory (No. Y0D1051F211).

Conflict of Interest

The authors declare no conflict of interest.

Data Availability Statement

The data that support the findings of this study are available in the supplementary material of this article.

Supplementary Information

The supporting information is available free of charge.

Figures S1 to S8: representative demonstration for the tunneling layer transfer process, electrical measurement, tunneling barrier calculation and so on. (PDF)

Supplementary video: Printing process of Ga₂O₃ tunneling layer.

Reference

1. Radisavljevic, B., Radenovic, A., Brivio, J. et al. Single-layer MoS₂ transistors. *Nat. Nanotechnol.* **6**, 147–150 (2011). <https://doi.org/10.1038/nnano.2010.279>
2. Liu, Y., Duan, X., Shin, HJ. et al. Promises and prospects of two-dimensional transistors. *Nature* **591**, 43–53 (2021). <https://doi.org/10.1038/s41586-021-03339-z>
3. Allain, A., Kang, J., Banerjee, K. et al. Electrical contacts to two-dimensional semiconductors. *Nature Mater.* **14**, 1195–1205 (2015). <https://doi.org/10.1038/nmat4452>
4. Li, Z. et al. Efficient strain modulation of 2D materials via polymer encapsulation. *Nat. Commun.* **11**, 1151 (2020). <https://doi.org/10.1038/s41467-020-15023-3>
5. Wang, Y., Sarkar, S., Yan, H. & Chhowalla, M. Critical challenges in the development of electronics based on two-dimensional transition metal dichalcogenides. *Nat. Electron.* **7**, 638–645 (2024) doi:10.1038/s41928-024-01210-3.

6. Liu, Y. *et al.* Low-resistance metal contacts to encapsulated semiconductor monolayers with long transfer length. *Nat. Electron.* **5**, 579–585 (2022).
<https://doi.org/10.1038/s41928-022-00808-9>
7. Wang, L. Hu, Y. Kim, S.Y. *et al.* Origins of Fermi Level Pinning for Ni and Ag Metal Contacts on Tungsten Dichalcogenides. *ACS Nano* **17** (20), 20353-20365 (2023) <https://pubs.acs.org/doi/10.1021/acsnano.3c06494>.
8. Jiang, J., Xu, L., Du, L. *et al.* Yttrium-doping-induced metallization of molybdenum disulfide for ohmic contacts in two-dimensional transistors. *Nat. Electron.* **7**, 545–556 (2024). <https://doi.org/10.1038/s41928-024-01176-2>
9. Pack, J. *et al.* Charge-transfer contacts for the measurement of correlated states in high-mobility WSe₂. *Nat. Nanotechnol.* **19**, 948–954 (2024).
<https://doi.org/10.1038/s41565-024-01702-5>
14. Jung, Y., Choi, M.S., Nipane, A. *et al.* Transferred via contacts as a platform for ideal two-dimensional transistors. *Nat. Electron.* **2**, 187–194 (2019).
<https://doi.org/10.1038/s41928-019-0245-y>
10. Wang, Y., Kim, J.C., Wu, R.J. *et al.* Van der Waals contacts between three-dimensional metals and two-dimensional semiconductors. *Nature* **568**, 70–74 (2019). <https://doi.org/10.1038/s41586-019-1052-3>
11. Shen, P.C., Su, C., Lin, Y. *et al.* Ultralow contact resistance between semimetal and monolayer semiconductors. *Nature* **593**, 211–217 (2021).
<https://doi.org/10.1038/s41586-021-03472-9>
12. Li, W., Gong, X., Yu, Z. *et al.* Approaching the quantum limit in two-dimensional

semiconductor contacts. *Nature* **613**, 274–279 (2023).

<https://doi.org/10.1038/s41586-022-05431-4>

- Liu, Y., Cheng, H-C., Yang, S., et. Toward Barrier Free Contact to Molybdenum Disulfide Using Graphene Electrodes. *Nano Lett.* **15** (5), 3030-3034. (2015) DOI: 10.1021/nl504957p
15. Dankert, A., Langouche, L., Kamalakar, M. V. & Dash, S. P. High-Performance Molybdenum Disulfide Field-Effect Transistors with Spin Tunnel Contacts. *ACS Nano* **8**, 476–482 (2014). DOI: 10.1021/nn404961e
16. McDonnell, S., Brennan, B., Azcatl, A., et. al. HfO₂ on MoS₂ by Atomic Layer Deposition: Adsorption Mechanisms and Thickness Scalability. *ACS Nano* **7** (11), 10354-10361. (2013) <https://pubs.acs.org/doi/10.1021/nn404775u>.
17. Lee, S., Tang, A., Aloni, S. & Philip Wong, H.-S. Statistical Study on the Schottky Barrier Reduction of Tunneling Contacts to CVD Synthesized MoS₂. *Nano Lett.* **16**, 276–281 (2016). DOI: 10.1021/acs.nanolett.5b03727
18. Wang, J. et al. High Mobility MoS₂ Transistor with Low Schottky Barrier Contact by Using Atomic Thick h-BN as a Tunneling Layer. *Adv. Mater.* **28**, 8302–8308 (2016). <https://doi.org/10.1002/adma.201602757>
19. Xu, B. et al. Alleviation of Schottky barrier heights at TMDs/metal interfaces with a tunneling layer of semiconducting InSe nanoflake. *Appl. Surf. Sci.* **636**, 157853 (2023). <https://doi.org/10.1016/j.apsusc.2023.157853>
20. Kim, J. et al. Improved Contact Resistance by a Single Atomic Layer Tunneling Effect in WS₂/MoTe₂ Heterostructures. *Adv. Sci.* **8**, 2100102 (2021).

<https://doi.org/10.1002/advs.202100102>

21. Phan, N. A. N. *et al.* Enhanced Performance of WS₂ Field-Effect Transistor through Mono and Bilayer h-BN Tunneling Contacts. *Small* **18**, 2105753 (2022). <https://doi.org/10.1002/sml.202105753>
22. Kim, K.S., Kwon, J., Ryu, H. *et al.* The future of two-dimensional semiconductors beyond Moore's law. *Nat. Nanotechnol.* **19**, 895–906 (2024). <https://doi.org/10.1038/s41565-024-01695-1>
23. Wang, S., Liu, X., Xu, M. *et al.* Two-dimensional devices and integration towards the silicon lines. *Nat. Mater.* **21**, 1225–1239 (2022). <https://doi.org/10.1038/s41563-022-01383-2>
24. Syed, N. *et al.* Wafer-Sized Ultrathin Gallium and Indium Nitride Nanosheets through the Ammonolysis of Liquid Metal Derived Oxides. *J. Am. Chem. Soc.* **141**, 104–108 (2019). DOI: 10.1021/jacs.8b11483
25. Li, J. *et al.* Template Approach to Large-Area Non-layered Ga-Group Two-Dimensional Crystals from Printed Skin of Liquid Gallium. *Chem. Mater.* **33**, 4568–4577 (2021). DOI: 10.1021/acs.chemmater.1c00999
26. Yi, K. *et al.* Van der Waals Encapsulation by Ultrathin Oxide for Air-Sensitive 2D Materials. *Adv. Mater.* 2403494 (2024) doi:10.1002/adma.202403494.
27. Cho, H., Pujar, P., Cho, Y. I., Hong, S. & Kim, S. Ultrathin Al-Assisted Al₂O₃ Passivation Layer for High-Stability Tungsten Diselenide Transistors and Their Ambipolar Inverter. *Adv. Electron. Mater.* **8**, 2101012 (2022). <https://doi.org/10.1002/aelm.202101012>

28. Ryu, H. *et al.* Fluorinated Graphene Contacts and Passivation Layer for MoS₂ Field Effect Transistors. *Adv. Electron. Mater.* **8**, 2101370 (2022). <https://doi.org/10.1002/aelm.202101370>
29. Wurdack, M. *et al.* Ultrathin Ga₂O₃ Glass: A Large-Scale Passivation and Protection Material for Monolayer WS₂. *Adv. Mater.* **33**, 2005732 (2021).
30. Kong, M. *et al.* Ambient printing of native oxides for ultrathin transparent flexible circuit boards. *Science* **385**, 731–737 (2024).
29. Yang, FS., Li, M., Lee, MP. *et al.* Oxidation-boosted charge trapping in ultra-sensitive van der Waals materials for artificial synaptic features. *Nat. Commun.* **11**, 2972 (2020). <https://doi.org/10.1038/s41467-020-16766-9>
30. Song, S., Hong, W.-K., Kwon, S.-S. & Lee, T. Passivation effects on ZnO nanowire field effect transistors under oxygen, ambient, and vacuum environments. *Appl. Phys. Lett.* **92**, 263109 (2008). <https://doi.org/10.1063/1.2955512>
31. Yang, L. *et al.* Chloride Molecular Doping Technique on 2D Materials: WS₂ and MoS₂. *Nano Lett.* **14**, 6275–6280 (2014). DOI: 10.1021/nl502603d
32. Khalil, H. M. W., Khan, M. F., Eom, J. & Noh, H. Highly Stable and Tunable Chemical Doping of Multilayer WS₂ Field Effect Transistor: Reduction in Contact Resistance. *ACS Appl. Mater. & Inter.* **7**.42, 23589-23596. (2015) DOI: 10.1021/acsami.5b06825
33. Iqbal, M. W. *et al.* Tailoring the electrical and photo-electrical properties of a WS₂ field effect transistor by selective n-type chemical doping. *RSC Adv.* **6**, 24675–24682 (2016). DOI:<https://doi.org/10.1039/C6RA02390H>

34. Jiang, J. *et al.* A Facile and Effective Method for Patching Sulfur Vacancies of WS₂ via Nitrogen Plasma Treatment. *Small* **15**, 1901791. (2019) <https://doi.org/10.1002/sml.201901791>.
35. Park, W. *et al.* Complementary Unipolar WS₂ Field-Effect Transistors Using Fermi-Level Depinning Layers. *Adv. Electron. Mater.* **2**, 1500278. (2016). doi: 10.1002/aelm.201500278
36. Yeh, C.-H. *et al.* Scalable T-Gate Aligned Gr–WS₂–Gr Radio-Frequency Field-Effect Transistors. *ACS Appl. Electron. Mater.* **2**, 3898–3905 (2020). DOI: 10.1021/acsaelm.0c00742
37. Kim, Y. J., Park, W., Yang, J. H., Kim, Y. & Lee, B. H. Contact Resistance Reduction of WS₂ FETs Using High-Pressure Hydrogen Annealing. *IEEEJ. Electron Devices Soc.* **6**, 164–168 (2018). DOI:10.1109/JEDS.2017.2781250
38. Liu, M. *et al.* Enhanced carrier transport by transition metal doping in WS₂ field effect transistors. *Nanoscale* **12**, 17253–17264 (2020). <https://doi.org/10.1039/D0NR01573C>
39. Ju, S. *et al.* Electrical contact properties between Yb and few-layer WS₂. *Appl. Phys. Lett.* **120**(25): 253505. (2022) <https://doi.org/10.1063/5.0095493>
42. Banerjee, S., Luginsland, J. & Zhang, P. A Two Dimensional Tunneling Resistance Transmission Line Model for Nanoscale Parallel Electrical Contacts. *Sci. Rep.* **9**, 14484 (2019). <https://doi.org/10.1038/s41598-019-50934-2>
40. Shi, X. *et al.* Improved Self-Heating in Short-Channel Monolayer WS₂ Transistors with High-Thermal Conductivity BeO Dielectrics. *Nano Lett.* **22** (18), 7667-7673

(2022) doi:10.1021/acs.nanolett.2c02901.

41. Cui, X., Lee, G.H., Kim, Y. et al. Multi-terminal transport measurements of MoS₂ using a van der Waals heterostructure device platform. *Nat. Nanotech.* **10**, 534–540 (2015). <https://doi.org/10.1038/nnano.2015.70>
42. Gebhard, F. *The Mott Metal-Insulator Transition: Models and Methods* (ed. Gebhard, F.) 1–48 (Springer Berlin Heidelberg, Berlin, Heidelberg, 1997). doi:10.1007/3-540-14858-2_1.
43. Ovchinnikov, D., Allain, A., Huang, Y.-S., Dumcenco, D. & Kis, A. Electrical Transport Properties of Single-Layer WS₂. *ACS Nano* **8** (8), 8174-8181 (2014). doi:10.1021/nn502362b.
44. Wan, Y., Li, E., Yu, Z. et al. Low-defect-density WS₂ by hydroxide vapor phase deposition. *Nat. Commun.* **13**, 4149 (2022). <https://doi.org/10.1038/s41467-022-31886-0>
45. Chen, J.H., Jang, C., Adam, S. et al. Charged-impurity scattering in graphene. *Nature Phys.* **4**, 377–381 (2008). <https://doi.org/10.1038/nphys935>
46. Kaasbjerg, K., Thygesen, K. S. & Jauho, A.-P. Acoustic phonon limited mobility in two-dimensional semiconductors: Deformation potential and piezoelectric scattering in monolayer MoS₂ from first principles. *Phys. Rev. B* **87**, 235312 (2013). <https://doi.org/10.1103/PhysRevB.87.235312>
47. Farmanbar, M. & Brocks, G. Controlling the Schottky barrier at MoS₂/metal contacts by inserting a BN monolayer. *Phys. Rev. B* **91**, 161304 (2015). <https://doi.org/10.1103/PhysRevB.91.161304>

48. Chen, J.-R. *et al.* Control of Schottky Barriers in Single Layer MoS₂ Transistors with Ferromagnetic Contacts. *Nano Lett.* **13**, 3106–3110 (2013). DOI: 10.1021/nl4010157
49. Wen, X. *et al.* ZrTe₂ Compound Dirac Semimetal Contacts for High-Performance MoS₂ Transistors. *Nano Lett.* **23**, 8419–8425 (2023). DOI: 10.1021/acs.nanolett.3c01554
50. Chiu, F.-C. A Review on Conduction Mechanisms in Dielectric Films. *Adv. Mater. Sci. Eng.* **2014**, 578168 (2014). <https://doi.org/10.1155/2014/578168>
51. Retamal, J. R. D., Periyanaounder, D., Ke, J.-J., Tsai, M.-L. & He, J.-H. Charge carrier injection and transport engineering in two-dimensional transition metal dichalcogenides. *Chem. Sci.* **9**, 7727–7745 (2018). DOI: <https://doi.org/10.1039/C8SC02609B>
52. van Bremen, R., Vonk, K. & Zandvliet, H. J. W. Environmentally Controlled Charge Carrier Injection Mechanisms of Metal/WS₂ Junctions. *J. Phys. Chem. Lett.* **10** (10), 2578-2584 DOI: 10.1021/acs.jpcllett.9b00862